Supplementary Information for

Quantifying Static Capacity Losses in Solid-State Battery Composites via Coulometric Titration Comparison

Kilian Vettori[a†*], *Maximilian Kissel*[a†], *Daniel Wagner*[a], *Steffen Schröder*[b] *and Jürgen Janek*[a*]

[a]Institute of Physical Chemistry & Center for Materials Research (ZfM/LaMa), Justus Liebig University Giessen, Heinrich-Buff-Ring 17, 35392 Giessen, Germany.

[b]Institute of Experimental Physics I & Center for Materials Research (ZfM/LaMa), Justus Liebig-University Giessen, Heinrich-Buff-Ring 16, 35392 Giessen, Germany

[†] These authors contributed equally.

Table of Contents

1. Experimental details

For all experiments, single crystalline $LiNi_{0.82}Co_{0.11}Mn_{0.07}$ (MSE Supplies LLC, Tucson, AZ, USA) was used as cathode active material (CAM). This material was further used in solid state battery cells (SSB) and liquid electrolyte battery cells (LIB). Cell assembly and storage were done in an argon-filled glovebox, with oxygen residues of $p(O_2)/p < 1.0$ ppm and water residues of $p(H_2O)/p < 1.0$ ppm.

1.1. SSB assembly

The composites were mixed in a mini vibrating mill (Pulverisette 23 from Fritsch GmbH, Idar-Oberstein, Germany) using 6 ZrO_2 balls with 5 mm diameter at 30 Hz for 15 minutes. Commercially available Li_6PS_5Cl (Argyrodite-CSMP from Posco JK Solid Solution, South Korea) was used as catholyte without further modification. The composites had different mass ratios, while the total mass of 200 mg was kept constant. For certain composites, carbon nanofibers (product number 719781 from Sigma-Aldrich, Sainz Louis, MO, USA) were used as conductive additive.

For the electrochemical half cells, an in-house made cell casing was used, and the assembly followed a standardized protocol: First, 80 mg of Li_6PS_5Cl (NEI Corporation, Somerset, NJ, USA) were filled in the mold and pressed by hand. 15 mg of the prepared cathode composite were evenly distributed on top of the separator and pressed by hand. The cell was afterwards pressed uniaxially at 375 MPa for 3 min. Then, as anode, an indium foil (Alfa Aesar, 99.99%, 9 mm diameter, 100 µm thickness) and a lithium foil (China Energy Lithium, 6 mm diameter, 100 µm thickness) were placed on the bottom side of the separator.

1.2. LIB Assembly

For the preparation of LIB cathodes, a conventional tape-casting method was employed within Ar atmosphere. The slurry comprised a mixture of NCM, carbon, and binder at a weight ratio of 94:3:3, using N-methyl-2-pyrrolidone (NMP) as solvent and was cast onto aluminum foil. The materials used were NMP (Sigma-Aldrich Chemie GmbH, Steinheim, Germany), SuperP carbon (MSE Supplies LLC, Tucson, USA), and PVDF (Arkema France, Colombes Cedex, France) as binder.

Resulting cathodes had 12 mm diameter and were pressed at 200 MPa. Within the experiments different loadings from ~5-10 mg/cm^2 were used. Currents/C-rates were calculated based on a practical capacity of 200 mAh/g, resulting in areal capacities of ~1-2 mAh/cm^2. Low cathode loadings are desired for CTC as explained in the main text. For CTC, simple two-electrode setups are sufficient, if the anode potential is constant. Thus, coin cells were assembled from a lithium chip (MSE Supplies LLC, Tucson, USA) with a diameter of 14 mm and a thickness of 600 µm and a glass fiber (GF/D – Whatman, Global Life sciences solutions USA LLC, Marlborough, USA) and a Celgard® 2325 separator (Celgard LLC, Charlotte, North Carolina, USA) and the cathode. As LE, 70 µl of LP57 (EC:EMC 3:7 (wt) + 1 M LiPF6) (BASF SE, Ludwigshafen, Germany) was used.

1.3. Electrochemical protocols

For electrochemical testing a BCS-805 Battery Cycling System (Bio-Logic, Seyssinet-Pariset, France) was used. To obtain the LIB coulometric titration curve, two formation cycles with 0.1C were applied between 3.0 and 4.3 V. Then pulses were applied with either 0.1C for 10 min or 0.05C for 20 min with 2 h relaxation.

For CTC of the SSBs, the half cells were tested under a stack pressure of about 80 MPa at 25°C. After an initial OCV period of 6h, the half cells were subjected to a formation cycle at 0.05C. Then the cells were charged at 0.05C to 3.1/3.2/3.3/3.4/3.5 V *vs* In-InLi, each time followed by at least 8 h of OCV relaxation. As a last step, they were charged to 3.53 V *vs* In-InLi, held at this potential for 12 h as preparation for XRD.

The required time of titration measurements can in principle be shortened with a minimum limit for the potential change during relaxation dV/dt. This might be valuable to minimize effects of self discharge, *e.g.* for unstable electrolytes. It has to be noted that the application of such limits was not employed here, as the SE showed great stability and the dV/dt limits showed to be sensitive to fluctuations especially at the end of relaxations where dV/dt < ΔV from voltage noise.

1.4. XRD measurement and refinement

X-ray diffraction was conducted using an Empyrean 2 powder diffractometer (Malvern Panalytical) with a Cu source in reflection mode. The SSB pellets were extracted from the cell housing and measured in a dome containing Ar atmosphere. Topas software was used for

Rietveld refinement and a LaB_6 standard measurement was used to obtain the instrumental resolution functions. Due to height deviations of the pellets, a variable zero-error function was used for the different measurements. This height deviation is an explanation for the slight shift in peak position between the pristine sample and the inactive mass phase of the composites. Please refer to SI section S4 for discussion of measurements.

2. Discussion of Assumptions and Errors during CTC

This chapter deals with uncertainties within the applied CTC procedure. First, the assumption of completely connected active material in LIBs is tested, then the important errors of the titration curve of the LIB reference are discussed in detail. Finally, the errors entering the CTC formulas are quantitatively estimated.

2.1. Assumption of complete connection of CAM in LIBs

To test this, we have applied a slow 0.05C charge up to 5.0 V to a pristine cathode. The total observed charge after an included hold at 5.0 V reveals a capacity above the theoretical one (indicated by grey dashed line in Fig S1).

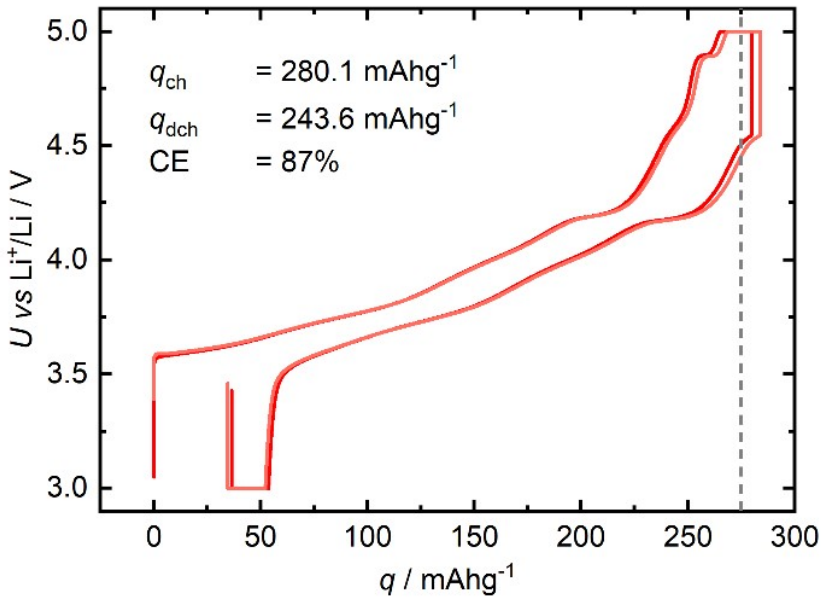

Fig S1: Dis-/charge curve of first cycle (0.05C + 4 h hold at 5 V and 24 h hold at 3 V) for two half cells (LIB). The observed specific capacity q exceeds the theoretical capacity indicated by the grey dashed line.

The observed charge certainly also contains contributions of parasitic currents and self-discharge which are difficult to quantify. Nevertheless, we believe the assumption of complete connection is justified as complete delithiation is kinetically hindered but capacities close to theoretical capacity are observed. Furthermore, the reference measurement could also have active mass utilizations below 100%, then all other measurements would show utilizations based on this reference. Thus, also a comparison among different SSB cells could be meaningful.

2.2. Suitable materials for CTC

In principle, CTC is suitable for all insertion materials that show potential evolution in near-equilibrium conditions when the stochiometry of the inserted species is varied. This applies to many active materials in various battery chemistries, most prominently layered oxides from the NCM family or $LiCoO_2$ (LCO)[1] which show solid solution behaviour over wide composition ranges.

As mentioned in the main text, the comparison of titration curves is more complicated for materials exhibiting extended voltage plateaus, where changes in stoichiometry lead to minimal variation in potential. This behavior, characteristic of two-phase reactions and staging phenomena, limits the sensitivity of voltage-based analyses to incremental composition changes. This is the case for $LiFePO_4$ (LFP)[2], $Li_4Ti_5O_{12}$ (LTO)[3] or $Na_3V_2(PO_4)_3$ (NVP)[4] exhibiting large 2-phase regions or hard carbon (HC)[5] anodes for Na-ion batteries, where a large voltage plateau due to Na insertion into nanoporous regions is observed. For such materials, suitable voltage windows (extending over the voltage plateaus) have to be chosen so that an evaluation with CTC becomes meaningful.

For conversion-type materials, voltage hysteresis, multi-electron processes, and structural rearrangements further decouple voltage response from stoichiometry,[6] as *e.g.* observed for lithium reaction with transition metal oxides such as CoO/Co_3O_4 or Fe_2O_3.

2.3. Error estimation for titration curves

For a coulometric titration curve the relaxed potentials after titration, *i.e.*, constant current steps, are measured and plotted against the obtained charge. The error handling of such titration curves

has not been done in detail in literature to the best of our knowledge but is very relevant especially for CTC. Hence, the following sections discuss uncertainties of coulometric titration during charging of NCM. Here, we present our approach, available as python script to be reused by other researchers and give multiple suggestions on how to improve the procedure further.

2.3.1. Discussion on potential uncertainties

For the titration curve equilibrated potentials (OCP) are recorded. These should be possibly free from contributions of other electrodes (best is 3-electrode setup). Here, we discuss several influences on the potential. First, ongoing lithiation of the CAM, changing the equilibrium potential and SoC (self-discharge), *e.g.* due to degradation of Li-containing compounds, in the following denoted by I_{sd}. Second, incomplete relaxation, meaning that a lithium concentration gradient from the CAM particle surfaces to particle centers leads to a diffusion controlled potential change. Additionally, we account for the instrument error of the potentiostat.

2.3.1.1. Instrument error

Instrument errors can be considered small since modern potentiostats measure currents and potentials with very high precision. For instance, the used BCS-805 Battery Cycling System (Bio-Logic, Seyssinet-Pariset, France) measures potentials with an accuracy of at least $\pm$ 0.01% of the measured value $\pm$ 0.3 mV and currents with an accuracy of 0.05% $\pm$ 0.015% of the current range.[7] With an average voltage $\bar{U} \approx 3.7\ V$ one calculates:

$$\delta U_{instr} = \pm\ 0.01\%\ U \pm 0.3\ mV \approx 0.7\ mV\ (for\ \bar{U} = 3.7\ V) \qquad (1)$$

2.3.1.2. Incomplete relaxation and self-discharge

To gain an understanding of relaxation during titration, we have plotted dU/dt of an exemplary LIB titration curve at the end of relaxation steps over OCP in Fig S2. Fig S2a reveals that dU/dt is very dependent on the evaluation time. Even when the last 600 s of 2 h of relaxation (grey datapoints) are linearly fitted, all dU/dt values are below zero and during discharge above zero, indicating not completely equilibrated concentration gradients. Fig S2b shows interpolated and

smoothed dU/dt over OCP curves for charge and discharge, corresponding to the blue datapoints in Fig S2a. The orange curve is their average.

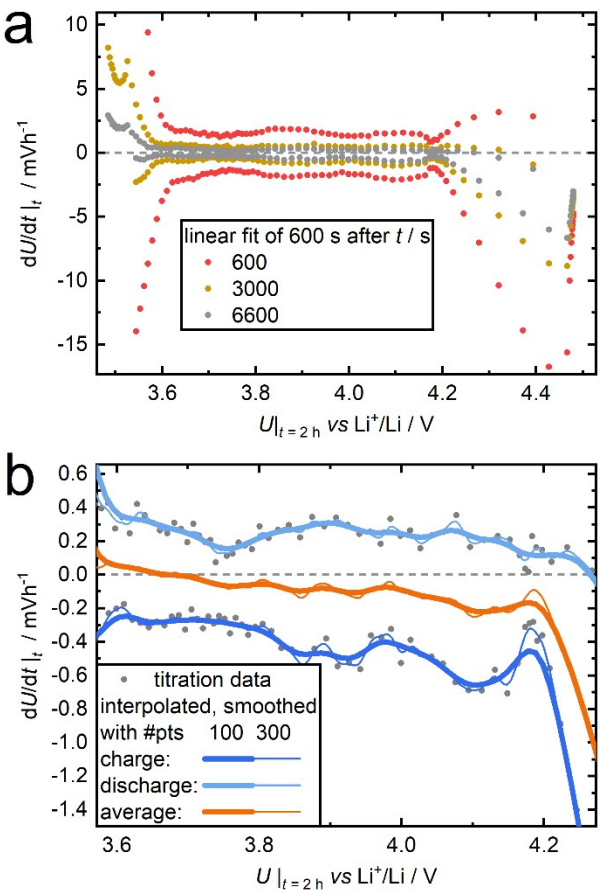

Fig S2: a) Change in potential in time dU/dt after various evaluation times during relaxation in a LIB. Positive values are from discharge, negative from charge. Deviation from zero indicates ongoing changes in lithium concentration at the particle surfaces. b) interpolated and smoothed dU/dt curves and their average (orange curve). Thick lines show interpolation with 100 datapoints and thin lines with 300.

The final dU/dt after charge contains a contribution from incomplete relaxation $\frac{\partial U}{\partial t}^{relax}$ and from self-discharge $\frac{\partial U}{\partial t}^{sd}$, both with negative signs (opposite sign of $\frac{\partial U}{\partial t}^{relax}$ for discharge). Calculating the average between dU/dt after charge and discharge (for the same potential/SoC) allows to separate $\frac{\partial U}{\partial t}^{sd}$ (Eq 2). The value can be used to calculate $\frac{\partial U}{\partial t}^{relax}$ according to Eq 3.

$$\frac{\partial U}{\partial t}^{sd} \approx \left(\frac{\partial U}{\partial t}\bigg|_{end\ of\ charge} + \frac{\partial U}{\partial t}\bigg|_{end\ of\ discharge} \right)/2 \tag{2}$$

$$\frac{\partial U}{\partial t}^{relax} \approx \frac{\partial U}{\partial t}\bigg|_{end\ of\ charge} - \frac{\partial U}{\partial t}^{sd} \tag{3}$$

For calculation of a self-discharge current, which also affects the measured charge during coulometric titration, please refer to SI section 2.2.2.2. The following equations show how U errors are calculated from both dU/dt contributions.

$$\delta U_{sd} \approx \frac{\partial U}{\partial t}^{sd} \cdot t_{relax} \tag{4}$$

$$\delta U_{relax} \approx \frac{\partial U}{\partial t}^{relax} \cdot t_{relax} \cdot f_{relax} \tag{5}$$

Here, we multiplied the potential change from self-discharge with the relaxation time t_{relax} to estimate the influence of self discharge after one titration step (Eq 4). $\frac{\partial U}{\partial t}^{relax}$ is multiplied with time t_{relax} which is scaled by an arbitrary factor f_{relax}, *e.g.* 2 (Eq 5). This factor assumes that the ongoing (linear) relaxation would need more time to equilibrate. For our well relaxed potential curves this appears reasonable but if the electrode of interest suffers from slow kinetics or the aim is to save time, then other more sophisticated extrapolations for the relaxed potentials are required.

To summarize: For the titration curve we used a symmetric statistical error due to the instrument δU_{instr} and a negative-only contribution due incomplete relaxation δU_{relax} and a positive-only

contribution δU_{sd} due to self-discharge. Care must be taken as these contributions depend on the sign of I_{pol}.

2.3.2. Discussion on charge uncertainties

This leads us to the estimation of charge uncertainties. If galvanostatic steps with identical current I_{pol} and time t_{pol} after initial charge Q_0 are applied, then the charge Q steps between datapoints are actually constant but still contain errors. These errors are in fact cumulative as also the total charge Q is the sum of all titration steps. The charge of step *i* can be expressed by Eq 6.

$$Q_i = Q_0 + \sum_1^i t_{pol} \cdot I_{pol} \tag{6}$$

This charge, as already mentioned, actually contains contributions from Faradaic efficiencies $FE \neq 1$ and self discharge current I_{sd} as shown in Eq 7.

$$Q_i = Q_0 + \sum_1^i t_{pol} \cdot I_{pol} \cdot FE - (t_{pol} + t_{relax}) \cdot I_{sd} \tag{7}$$

We suggest here an approach, where these additional contributions are estimated and summarized within errors of the actual charge Q. For our experiments we decided to assume $FE = 1$, as we believe we captured most of parasitic currents by I_{sd}. The important quantities are then Q_0, I_{pol} and I_{sd}.

2.3.2.1. Uncertainty of I_{pol}

The uncertainty of I_{pol} is given by the instrument error of the potentiostat[7] and results in an error in measured charge Q. For our titration settings ($I_{pol} = 52.5\ \mu A, I_{range} = 1\ mA, t_{pol} = 20\ min$) the errors can be calculated:

$$\delta I_{instr} = \pm\, 0.05\%\; I_{pol} \pm 0.015\%\; I_{range} \approx 0.18\ \mu A \tag{8}$$

$$\delta Q_{instr} = \delta I_{instr} \cdot t_{pol} \approx 0.06\ \mu Ah \tag{9}$$

2.3.2.2. Self-discharge current I_{sd}

Based on Fig S2 one can estimate I_{sd}. This represents a slightly modified version for a quantification of I_{sd} compared to common approaches which are well described in numerous publications.[8,9] There, much longer relaxation times are used and thus dU/dt is assumed to be only due to I_{sd}. Here, we chose an approach utilizing the potential fading $\overline{\frac{\partial U}{\partial t}}^{sd}$ due to self-discharge and the slope of the titration curve itself.

$$I_{sd}(U) \approx \overline{\frac{\partial U}{\partial t}}^{sd}\Big|_U \cdot \frac{\partial q}{\partial U}\Big|_U \cdot m_{CAM} \tag{10}$$

With this equation, I_{sd} is estimated as shown in Fig S3. For our procedure, we allowed only $0 > \overline{\frac{\partial U}{\partial t}}^{sd} > \overline{\frac{\partial U}{\partial t}}^{sd,max}$, with $\overline{\frac{\partial U}{\partial t}}^{sd,max}$ being evaluated at 4.1 V to be 0.2 µV/s. At this potential the H2-H3 transformation and the according peak in dq/dU curves lead to large uncertainty and these high potentials are to be avoided for CTC. Further we estimate an average $\bar{I}_{sd}$ during the time of formation $t_{formation}$ in order to determine the initial Q error from I_{sd} simply via $\Delta Q_{sd,formation} = t_{formation} \cdot \bar{I}_{sd}$.

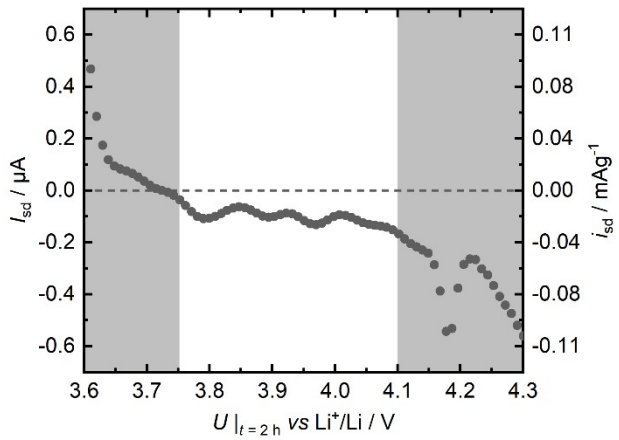

Fig S3: Self discharge current I_{sd} over potential as determined from Equation 10. Right axis shows i_{sd}, which is normalized to the mass of active material via $i_{sd} = I_{sd}/m_{CAM}$.

2.3.3. Mass uncertainty

The mass error is the most important factor when calculating $q = Q/m$. First, the effect of different cathode loadings in the LIB is discussed. Here, a higher cathode loading of the LIB can lead to more kinetic hindrance, and thus, errors in the reference titration curve. To show that the LIB reference used for CTC was unaffected from influence of loading, we performed coulometric titration on cathodes with varying loading as shown in Fig S4a.

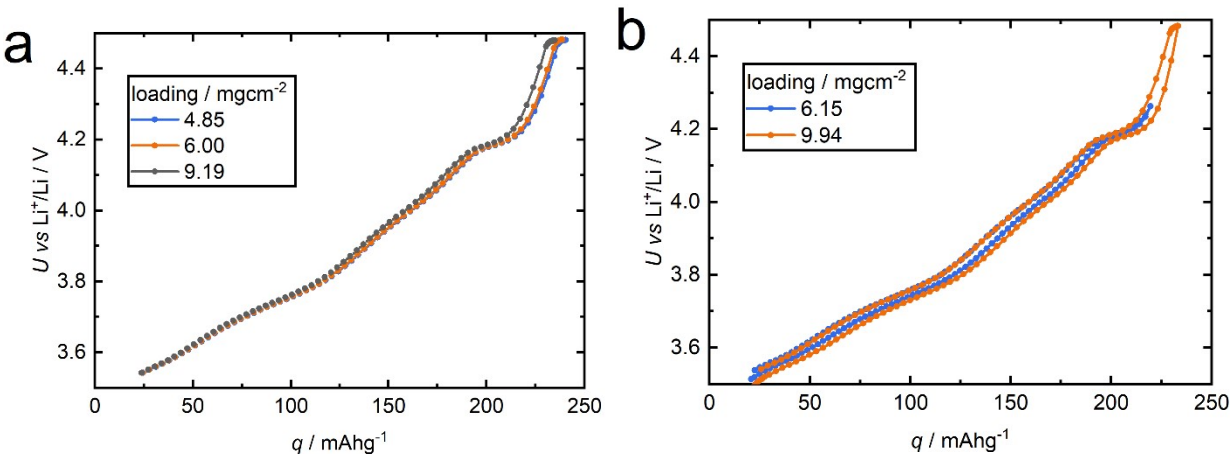

Fig S4: Titration curve (CAM in LIB) details. a) negligible effect of increasing cathode loadings below 4.2 V. b) Unexpected offset of titration curve between charge and discharge.

Here, the titration curves of the 6.00 mg/cm^2 cathode shows complete overlap with the 4.85 mg/cm^2 cathode. At 9.19 mg/cm^2 we observe a slight offset from the other curves, especially above 4.2 V. These potentials were avoided within the CTC protocol. The offset itself could be caused by incomplete relaxation but also by to static CAM loss, when CAM particles are no longer well connected within thick electrodes. As discussed in the main text, one deals with a tradeoff between high accuracy during weighing with increased loadings but more severe kinetic effects when concentration gradients within the cathode appear.

We also performed coulometric titration for charge and discharge and observed some hysteresis (Fig S4b), which deviates from the expected behavior of a characteristic titration curve. We believe this could be due to direction dependent phase transition behavior between the H2 and “quasi” H3 phase (seen in the orange curve) and due to lowered *FE* above 4.4 V when the cutoff potential is reached during polarization (orange and blue). In general, hysteresis behavior,

as *e.g.* during de-/lithiation of silicon, requires more sophisticated approaches. In our study, we chose to use titration curves during charge, as they show good overlap.

Regarding the mass error itself, we typically consider a weighing error of $\approx$ 0.1 mg if weighed masses are low. To understand the mass error during titration better, we used an experimental approach. Here, we explain the deviation of specific charges of N cells (with mass m_j and total charge Q_j at a given potential, here 4.15 V) from an average value $\bar{q}$ only by a mass error.

$$\delta m \approx \frac{1}{N}\sum_{j=1}^{N}\frac{Q_j}{\bar{q}} - m_j \tag{11}$$

For 6 tested cells we obtained $\delta m \approx$ 0.09 mg. With low loadings of $\approx$ 4 mg this corresponds to 2.3%.

2.3.4. Resulting uncertainties for titration curve

Based on the discussions above we included the following errors (Table 1) for the display of the titration curve of the LIB reference. Some of the errors are handled separately by the python script since this allows us to cancel errors for calculating ΔQ between two potentials. (see SI section 2.3)

Table 1: List of error contributions to titration curves (LIB)

error	type	sign
δU_{instr}	statistic	$\pm$
δU_{relax}	systematic	$-$ (for charge)
δU_{sd}	systematic	$+$ (for charge)
δQ_{instr}	statistic, cumulative	$\pm$
δQ_{sd}	systematic, cumulative	$-$
δm	statistic (systematic for q)	$\pm$

Since all q values of the titration curve are affected systematically, the listed uncertainties are added linearly. Here all charge contributions with same signs are simply added for $\delta Q_{\pm}$.

$$\Delta q_{\pm} \approx \frac{\delta Q_{\pm}}{m_{CAM}} + q \cdot \frac{\delta m}{m_{CAM}} \tag{12}$$

With this the following titration curve with error bands can be plotted in Fig S5.

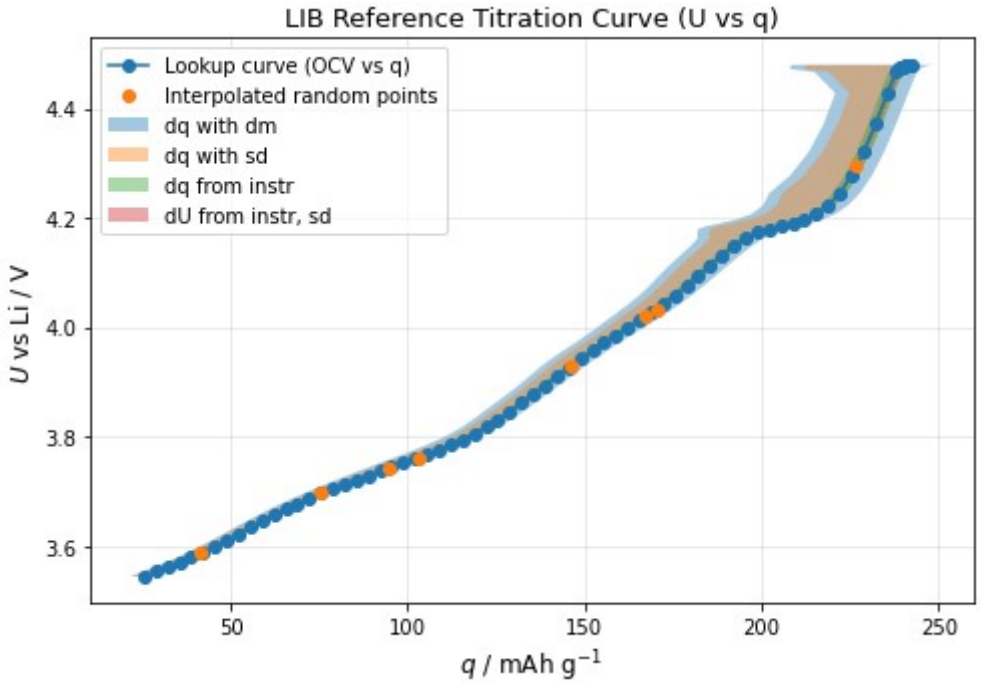

Fig S5: Resulting titration curve with error bands. This is also the output of the python script.

Here we see the inherent problem of cumulative errors for Q and the influence of mass error at higher specific charges. Especially at high SoC the influence of cumulative Q errors from self-discharge leads to large errors with negative sign. Also, potential plateaus as visible at around 4.2 V lead to increased uncertainty in q. This is expected as a slight change in potential corresponds to more charge if compared to steeper regions in the titration curve.

2.4. Errors of CTC

When applying CTC, a specific charge difference $^{\Delta q_{LIB}}$ between two potentials, $^{U_1} < {}^{U_2}$, is looked up from the titration curve shown in Fig S5. Since the q values share parts of their errors, these cancel out in the difference $^{\Delta q_{LIB}}$. In the following, the error propagation of the LIB reference titration curve and the "look-up" values of the SSB cell are discussed.

The active mass $^{m_{CAM.act}}$ of the SSB is calculated with Eq 13.

$$m_{CAM,act} = \frac{\Delta Q_{SSB}(U_1,U_2)}{\Delta q_{LIB}(U_1,U_2)} \qquad (13)$$

For our evaluation we estimated errors of $^{Q_{SSB}}$ and potentials from potentiostat accuracy and furthermore included a potential error with negative sign from incomplete relaxation again by

evaluating dU/dt at the end of relaxation periods. For δU_{relax} the relaxation time is scaled again by an arbitrary factor $f_{relax,SSB}$, in our case 1.63 (corresponding to additional 5 h of relaxation). We believe this captures the biggest error as slow kinetics pose the biggest challenge for SSBs. For calculating active mass utilization $\theta_{CAM,act}$ the weighing error enters as well.

The following table summarizes the errors for the SSB:

Table 2: Error contributions for SSB

error	type	sign
δU_{instr}	statistic	$\pm$
δU_{relax}	systematic	$-$ (for charge)
δQ_{instr}	statistic, cumulative	$\pm$
δm	statistic (systematic for q)	$\pm$

For eq 13 we have to lookup $\Delta q_{LIB}(U_1,U_2)$ from the titration curve. Here the errors of $U_1$and U_2 and the errors of the titration curve have to be propagated. In the following the quantities belong to the LIB (reference) curve by default and are indicated by SSB otherwise:

For the calculation of $\Delta q_{LIB}(U_1,U_2)$ itself we need to compute:

$$\Delta q = \frac{Q(U_2) - Q(U_1)}{m_{CAM,LIB}} \tag{14}$$

Then we check the sensitivity to perturbations in potential by the derivative at $U_1$and U_2.

$$A = \frac{dQ}{dU}(U_2),\ B = -\frac{dQ}{dU}(U_1) \tag{15}$$

The resulting errors for Q from $U_1$and U_2 ($i = 1,2$) are then dependent on the SSB and LIB measurement. Since both can contain "deterministic" contributions, positive and negative error contributions are denoted by $\pm$ in the index:

$$\delta U_{i,\pm} = \delta U_{i,SSB,\pm} + \delta U_{i,\pm} \tag{16}$$

(17)

$$\delta Q_{U,\pm} = A \cdot \delta U_{2,\pm} + B \cdot \delta U_{1,\pm}$$

Now the Q errors can be calculated. These are composed of $^{\delta Q_{U,\pm}}$ and the shared, cumulative contributions $^{\delta Q_{sd}}$, $^{\delta Q_{instr}}$. The latter cancel partially as shown in eq 18,19.

$$\delta Q_{+} = \delta Q_{U,+} + \delta Q_{instr}(U_2) - \delta Q_{instr}(U_1) \tag{18}$$

$$\delta Q_{-} = \delta Q_{U,-} + \delta Q_{instr}(U_2) - \delta Q_{instr}(U_1) + \delta Q_{sd}(U_2) - \delta Q_{sd}(U_1) \tag{19}$$

Now we need to introduce the mass error (δm) to get from Q data to specific capacities.

$$\delta q_m = \Delta q \cdot \frac{\delta m}{m_{AM}} \tag{20}$$

The final uncertainties in q are then:

$$\delta q_{\pm} = \frac{\delta Q_{\pm}}{m_{AM}} + \delta q_m \tag{21}$$

With the resulting (asymmetric) errors of $^{\Delta q_{LIB}(U_1,U_2)}$ and the errors of $^{\Delta Q_{SSB}(U_1,U_2)}$, the resulting error of $^{m_{CAM,act}}$ can be easily calculated (all Q errors for SSB are combined in $^{\delta Q_{SSB}}$):

$$\delta m_{CAM,act,\pm} = \pm \frac{Q_{SSB} \pm \delta Q_{SSB}}{q_{LIB} \mp \delta q_{\pm}} \mp \frac{Q_{SSB}}{q_{LIB}} \tag{22}$$

Eq 23 gives then the propagated error for $^{\theta_{CAM,act}}$

$$\delta \theta_{CAM,act,\pm} = \pm \frac{m_{CAM,act} \pm \delta m_{CAM,act,\pm}}{m_{CAM,tot} \mp \delta m_{CAM,tot}} \mp \frac{m_{CAM,act}}{m_{CAM,tot}} \tag{23}$$

3. Application of CTC to different SSB cells

The following section deals with the application of CTC to various SSB cells. The data evaluation is done with the Python script provided on github.[10]

3.1. Conversion to LIB reference potential

It might be necessary to use a different anode or reference electrode potential within the SSB compared to the reference titration measurement in LE. For the SSB cells of this study a typical In-InLi anode instead of pure Li metal was used for stability reasons. If SSB and LIB have varying reference electrodes, then the recorded cell voltages have to be converted to the LIB reference potential. This is only meaningful if the used reference potential within the SSB (anode or reference electrode) is stable and known.[11]

E.g., for the In-InLi two phase voltage plateau (employed in this study) an offset of +620 mV *vs* Li^+/Li is applied.[12] The accuracy of the offset can be checked by comparing the voltage of plateaus in titration curves of the investigated CAM or with more effort in additional cells of the type: SSB anode| SE | LIB anode (if applicable). A CAM titration curve becomes immediately distorted if the (relaxed) anode potential is not stable over the course of titration. To ensure stability, capacitively oversized anodes might be helpful.

3.2. Multiple potential steps

One approach to crosscheck results for $m_{CAM,act}$ or $\theta_{CAM,act}$, is the application of the CTC method at multiple relaxation potentials. Fig S6 shows exemplary output of the used python script for “good” and “bad” SSB. This labeling indicates that different cathode compositions and preparation protocols were used, for which varying degrees of CAM utilization are expected. For “good” SSB a mixture of CAM:SE:CNF with ratio of 70:30:1 and for “bad” SSB a mixture of CAM:SE of 60:40 was used. For more experimental details check section S1.1.

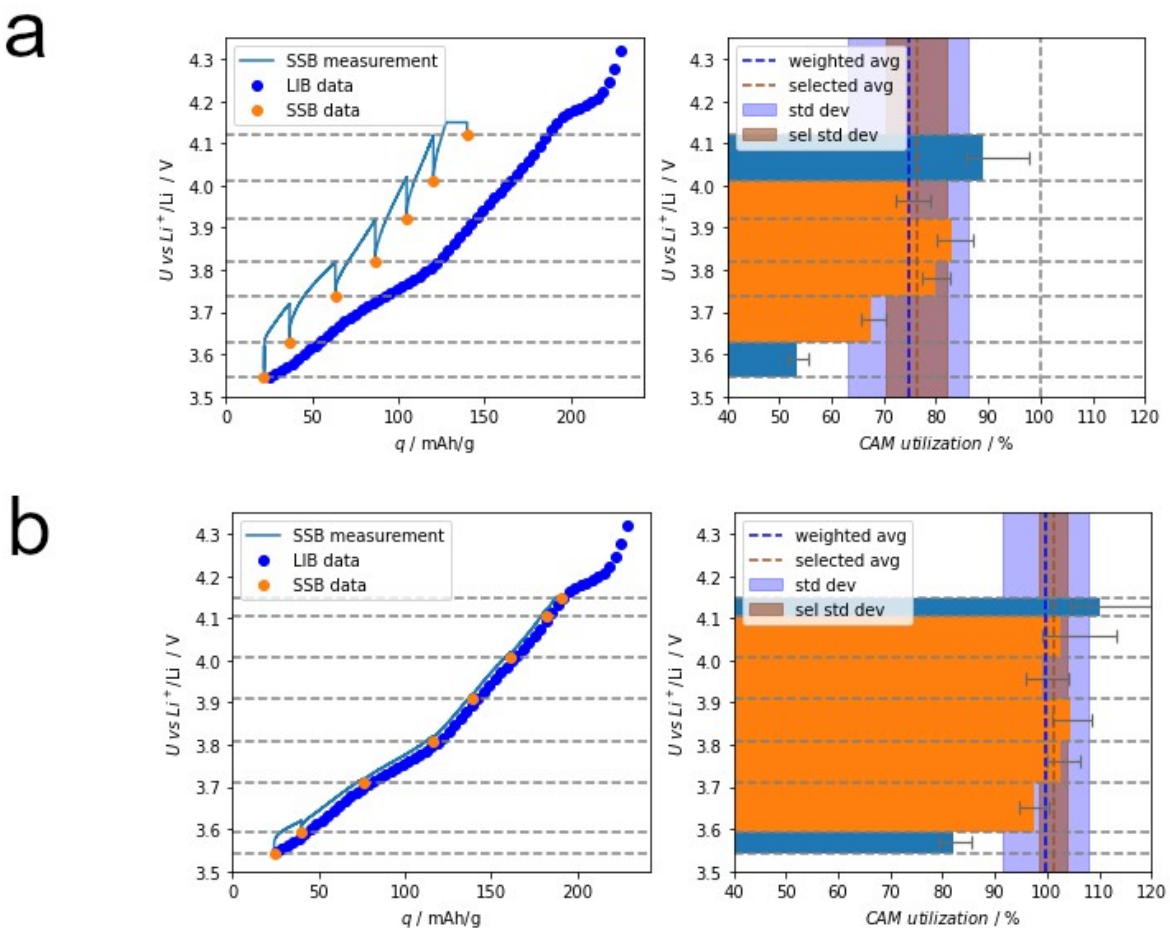

Fig S6: Result of Python script for CTC between different potential steps for a) "bad SSB" and b) "good SSB". Horizontal lines indicate voltage steps. In the right diagrams, each voltage step shows the corresponding $\theta_{CAM,act}$ result with error bars in grey. Averaged $\theta_{CAM,act}$ values are indicated via vertical dashed lines, standard deviations as transparent areas. A selected average is shown in orange/brown, for voltage steps with good kinetics.

For each potential step (indicated via horizontal lines) one result with uncertainty for $\theta_{CAM,act}$ can be calculated. Assuming constant $\theta_{CAM,act}$ during titration and fulfilled requirements for CTC (as discussed in the main text) means these $\theta_{CAM,act}$ can be averaged. The average and standard deviation for the exemplary "good" and "bad" SSB are shown in Fig S6 (right side) as dashed blue line and transparent blue. Additionally, we have incorporated the functionality in the python code to select a voltage window for a "selected" average. This can be useful to avoid voltage regions with bad kinetics (as for the presented SSBs at high and low potentials/SoC) or where side reactions are expected (*e.g.* if the SE in a given system shows reversible capacity). The

respective result is indicated as orange/brown in Fig S6, which is also the value given in the main text.

3.3. Various composite mixtures

We have tried different compositions to obtain a low CAM utilization in SSB composites and applied CTC to them. While the cells showed bad performance even during 0.05C cycling, CTC revealed that the capacity losses are mainly due to kinetics.

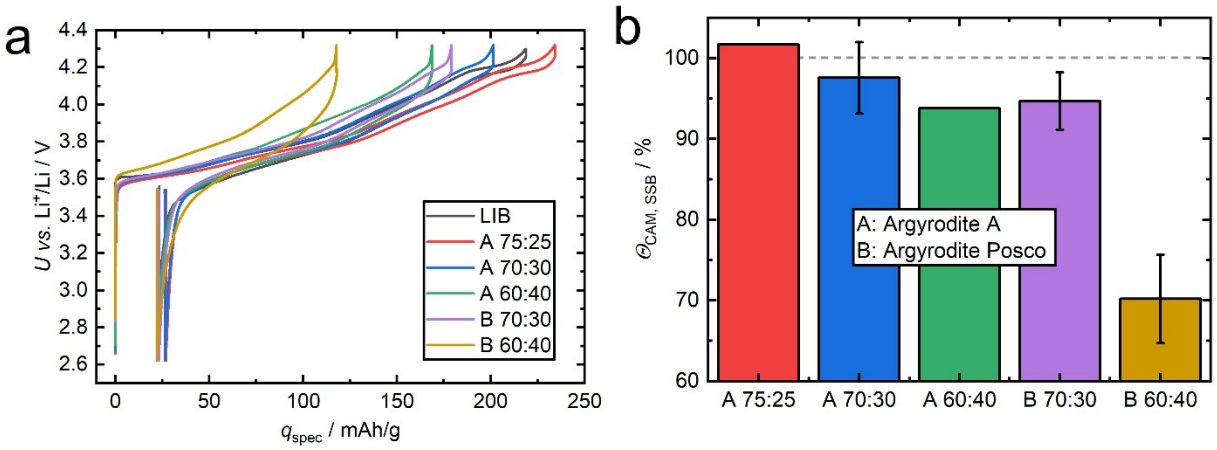

Fig S7: a) Performance during 1st charge of various SSB compositions. *A* and *B* refer to different Li_6PS_5Cl catholyte batches from different suppliers. b) Static CAM utilizations measured via CTC. Error bars here represent standard deviation of the average from multiple cells.

4. XRD measurements

Fig S8 shows complete diffractograms of pristine composite use for two good and bad SSBs each.

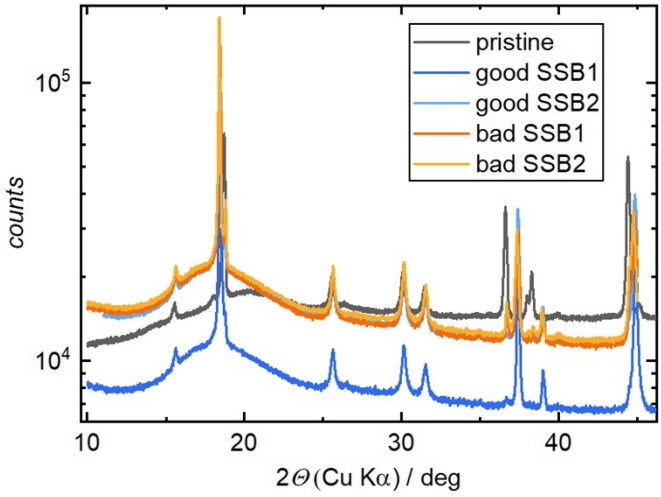

Fig S8: Complete diffractograms of composite pellets

To investigate the reflex shifting of NCM82 during delithiation, we conducted *in situ* XRD measurements using a Malvern Panalytical Empyrean 3 diffractometer equipped with a Molybdenum (Mo) source. The measurements were performed in transmission mode on a LIB in a pouch cell configuration, where no inactive material was expected. Two angle regions of interest are shown in Fig S9.

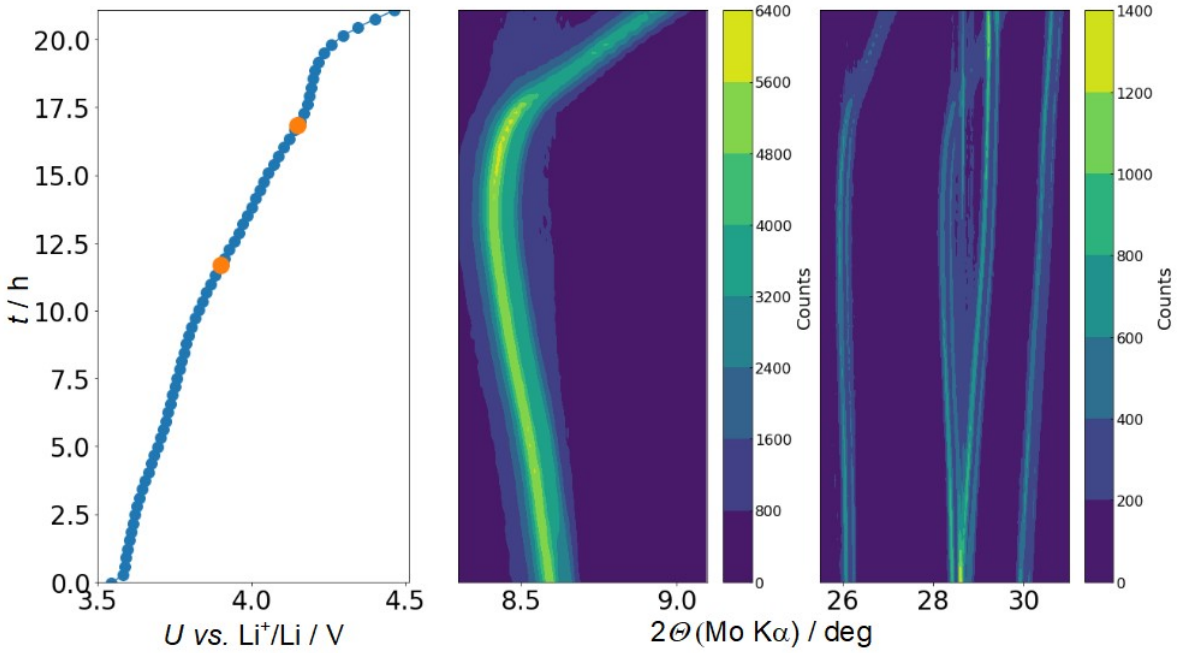

Fig S9: In-situ XRD measurement on LIB in pouch cell.

5. SSB performance normalized to $m_{CAM,act}$

With CTC it is possible to differentiate between static and kinetic capacity losses in SSBs.[13] For the two tested cells (good SSB and bad SSB) the 1st charges were normalized to the determined actual mass (meaning no static capacity losses). The remaining capacity loss is defined as "kinetic", shown as red in Fig S10.

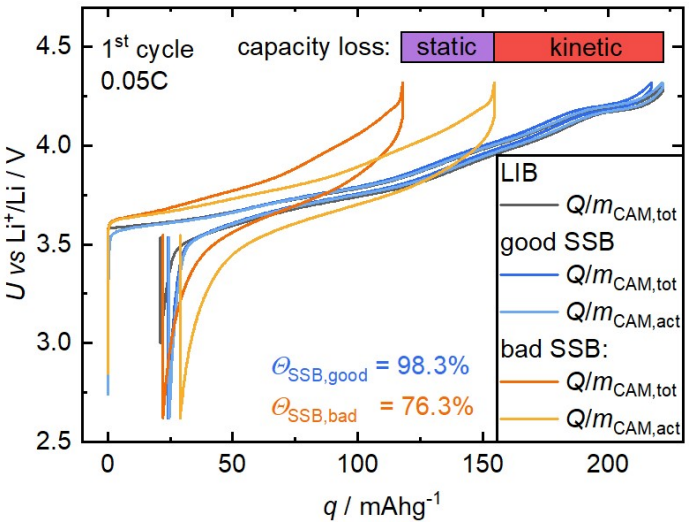

Fig S10: Schematic showing static and kinetic capacity losses. 1st cycle charge curves for SSBs are scaled by their actual mass of CAM (determined via CTC) and capacity losses for the "bad SSB" are indicated with purple and red.

6. Kinetic effects during LIB charging

To showcase how kinetic effects lead to a deviation of the charge curve from the titration curve, we have performed a rate test on the LIB. Fig S11 shows mainly increasing overpotentials but especially in regions of kinetic hindrance (low and high potentials) more complex behavior is observed.

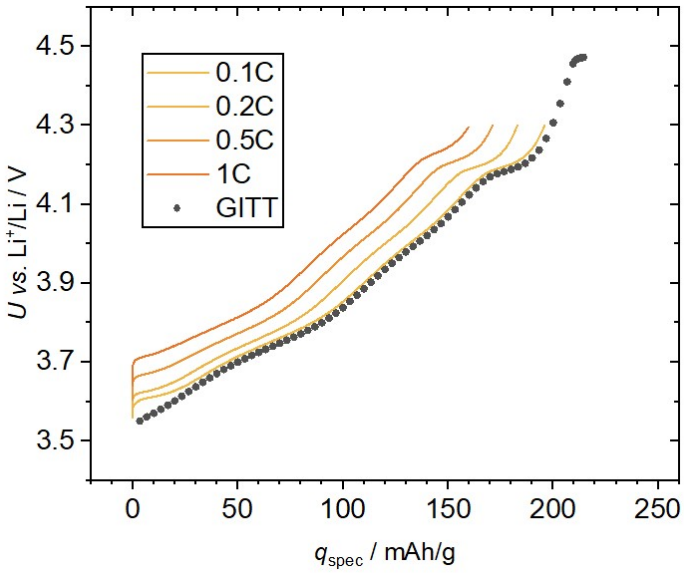

Fig S11: Kinetic effects on charge curve of LIB at different C-rates.

References

1 K. Mizushima, P. C. Jones, P. J. Wiseman and J. B. Goodenough, *Materials Research Bulletin*, 1980, **15**, 783–789.

2 A. K. Padhi, K. S. Nanjundaswamy and J. B. Goodenough, *J. Electrochem. Soc.*, 1997, **144**, 1188–1194.

3 T. Ohzuku, A. Ueda and N. Yamamoto, *J. Electrochem. Soc.*, 1995, **142**, 1431–1435.

4 G. Li, D. Jiang, H. Wang, X. Lan, H. Zhong and Y. Jiang, *Journal of Power Sources*, 2014, **265**, 325–334.

5 D. A. Stevens and J. R. Dahn, *Journal of The Electrochemical Society*, 2000, **147**, 1271.

6 J. Cabana, L. Monconduit, D. Larcher and M. R. Palacín, *Advanced Materials*, 2010, **22**, E170-92.

7 BioLogic, https://my.biologic.net/products/bcs-800-superseded/, (accessed 8 December 2025).

8 T. Roth, L. Streck, A. Graule, P. Niehoff and A. Jossen, *J. Electrochem. Soc.*, 2023, **170**, 20502.

9 L. Streck, T. Roth, P. Keil, B. Strehle, S. Ludmann and A. Jossen, *J. Electrochem. Soc.*, 2023, **170**, 40520.

10 Kilian Vettori, *CTC-data-analysis*, Zenodo. DOI: 10.5281/zenodo.17967963.

11 R. Zhang, A. Kondrakov, J. Janek and T. Brezesinski, *ACS Nano*, 2025. DOI: 10.1021/acsnano.5c17276.

12 A. L. Santhosha, Lukas Medenbach, Johannes R. Buchheim and Philipp Adelhelm, *Batteries & Supercaps*, 2019, **2**, 524–529.

13 M. Kissel, M. Schosland, J. Töws, D. Kalita, Y. Schneider, J. Kessler-Kühn, S. Schröder, J. Schubert, F. Frankenberg, A. Kwade, A. Bielefeld, F. H. Richter and J. Janek, *Advanced Energy Materials*, 2025, **15**. DOI: 10.1002/aenm.202405405.